Accepted Manuscript

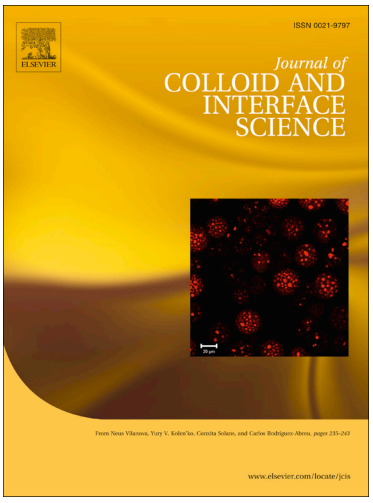

Nozzle-jet printed flexible field-effect transistor biosensor for high performance glucose detection

Kiesar Sideeq Bhat, Rafiq Ahmad, Jin-Young Yoo, Yoon-Bong Hahn

PII: S0021-9797(17)30803-2
DOI: http://dx.doi.org/10.1016/j.jcis.2017.07.037
Reference: YJCIS 22566

To appear in: *Journal of Colloid and Interface Science*

Received Date: 23 May 2017
Revised Date: 11 July 2017
Accepted Date: 13 July 2017

Please cite this article as: K. Sideeq Bhat, R. Ahmad, J-Y. Yoo, Y-B. Hahn, Nozzle-jet printed flexible field-effect transistor biosensor for high performance glucose detection, *Journal of Colloid and Interface Science* (2017), doi: http://dx.doi.org/10.1016/j.jcis.2017.07.037

This is a PDF file of an unedited manuscript that has been accepted for publication. As a service to our customers we are providing this early version of the manuscript. The manuscript will undergo copyediting, typesetting, and review of the resulting proof before it is published in its final form. Please note that during the production process errors may be discovered which could affect the content, and all legal disclaimers that apply to the journal pertain.

ACCEPTED MANUSCRIPT

Nozzle-jet printed flexible field-effect transistor biosensor for high performance glucose detection

Kiesar Sideeq Bhat, Rafiq Ahmad, Jin-Young Yoo and Yoon-Bong Hahn*

School of Semiconductor and Chemical Engineering, Nanomaterials Processing Research Center, Chonbuk National University, 567 Baekjedaero, Deokjin-gu, Jeonju-si, Jeollabuk-do, 54896, Republic of Korea.

* **Corresponding author**. Tel.: +82 63 2702439; Fax: +82 63 2702306

E-mail: ybhahn@chonbuk.ac.kr (Y. B. Hahn)

ACCEPTED MANUSCRIPT

ACCEPTED MANUSCRIPT

Abstract

Printable electronics is a subject of great interest for low-cost, facile and environmentally-friendly large scale device production. But, it still remains challenging for printable biosensor development. Herein, we present the fabrication of nozzle-jet printed flexible field-effect transistor (FET) glucose biosensor. The silver source-drain electrodes and ZnO seed layers were printed on flexible substrate by nozzle-jet printer followed by ZnO nanorods (ZnO NRs) synthesis and glucose oxidase (GOx) immobilization. Utilization of nozzle-jet printing methods resulted in highly reproducible electrodes with well-defined vertical grown ZnO NRs for high GOx loading and enhanced glucose sensing performance in a wide glucose detection range. The stability, anti-interference ability, reproducibility, reusability, and applicability in human serum samples were also assessed. Overall, biosensor fabrication using nozzle-jet printer will not only provide large scale production of highly reproducible electrodes but also reduce the fabrication cost. Additionally, printed electrodes can be modified accordingly for different analyte detection.

Keywords: Nozzle-jet printing; ZnO nanorods; field-effect transistor; glucose biosensor

ACCEPTED MANUSCRIPT

ACCEPTED MANUSCRIPT

1. Introduction

Diabetes mellitus is affecting human health worldwide. Especially, in developed countries diabetes mellitus has shown major complications such as increased risk of heart disease (2-3 times higher prevalence rate than nondiabetic), kidney failure (80% end-stage renal disease caused by diabetes), non-healing wounds (1.5-3.5 of lower limb amputations per 1000 diabetic persons per year), blindness (35% of diabetic patients suffer from retinopathy) and neurological conditions [1-4]. These metabolic disorders result from insulin deficiency, which affects blood glucose concentration levels (normal range is 4.4-6.6 mM). According to the World Health Organization (WHO), 1.5 million deaths were caused by diabetes in 2012 with additional 2.2 million related to higher than normal blood glucose levels. Addressing this problem, the World Health Day 2016 entitled "Beat Diabetes" was devoted to this disease [5]. Hence, accurate glucose detection is important for the treatment and management of diabetes. Different methods have been reported for glucose sensing i.e. Raman spectroscopy, optical and electrochemical [6-8]. Among them, electrochemical based sensing is particularly interesting because of the potential to create compact and low-cost devices.

Recently, field-effect transistor (FET) type biosensors have attracted considerable research interest, owing to the large current amplification and relatively high signal-to-noise ratio [9-14]. For FET based biosensors fabrication, semiconductors include carbon nanotubes [15], organic [16-20] and inorganic [21] have been largely applied to detect a wide range of analytes by monitoring the current changes [22, 23]. Biosensing with various nanostructured metal oxide based semiconductors has recently been reviewed [24-26].

ACCEPTED MANUSCRIPT

Among different nanostructured materials, ZnO is an unique material with excellent electrical property which has been widely used for the fabrication of low-cost sensors [27, 28]. High isoelectric point (IEP ~ 9.5) and large specific surface area of ZnO nanostructures make it appropriate for low IEPs proteins or enzymes immobilization at pH 7.4. Moreover, the ample available ZnO nanostructures including NRs, nanotubes, nanowires, nanoparticles, nanonails, nano-combs, nano-flake, hollow nano-spheres, etc. have been utilized for glucose biosensor fabrication [24-26, 29-34]. The ZnO NRs integrated FET has opened up a new route towards the development of high performance and efficient biosensors [35]. The sensing performances of biosensors are greatly affected by the attachment method used to attach nanostructures on the electrode surface [36-39]. For biosensor fabrication, directly-grown nanostructures on the electrode surface not only avoid the use of binders (reduce the catalytic activity by blocking the catalytic active sites when used to attach nanostructures on the electrode surface) but also provides stable electrodes with controlled surface morphology and large specific surface area for high amount of enzyme immobilization. Also, the directly-grown nanostructures on electrode surface directly transfer electrons to the electrode surface during enzymatic reactions [39].

Among different nanostructure deposition methods on electrode surface, inkjet-printing method is mainly used to deposit possible pattern on flexible substrates for facile, environmental-friendly, high-throughput, high-volume and low-cost electronic devices. This method possesses an attractive combination of spatial resolution, printing speed, reproducibility, modest capital cost and minimal waste. Furthermore, inkjet-printing allows the designed device pattern to be directly applied to the substrate and avoids dyes, masks, chemical etchants, and complications associated with other

ACCEPTED MANUSCRIPT

patterning approaches. Inkjet printing often in combination with other deposition/patterning approaches (i.e. spin coating/patterning, screen printing/patterning and plotter printing) have been used to fabricate numerous electronic devices (e.g., transistors and light emitting displays) on different substrates [40, 41] for inexpensive and large-area electronics such as in radio frequency identification tags (RFID's), flexible electrophoretic displays and artificial skins [42-44].

From the advent of the idea of printed electronics, inorganic semiconductors can be regarded as inexpensive, nontoxic and high quality oxide semiconductors. Printed inorganic semiconductor channel transistors can be produced either from an oxide precursor subsequently heated to obtain a high quality un-doped/doped oxide semiconductor [45-47] or from a dispersion of inorganic nanoparticles as a nano-ink [48-50]. However, high temperature processing of oxide precursor limits the choice of substrates and removes the possibility of using polymers/papers. In case of nano-inks, it is difficult to establish a smooth interface between the nanoparticulate channel and the dielectric [40]. The interface roughness influences the mobility, where rough interface with big agglomerates results in low mobilities and smooth interface with small agglomerates leads to high mobilities [51]. Hence, it is nearly impossible to obtain a satisfactory field-effect using printed nanoparticles. Also, the use of stabilizer molecules to get stable nanoparticle dispersions remains as a semi-insulating barrier between the particles that acts as charge traps, reduce mobility and switching speed of such devices [40].

Herein, we introduce a new approach to address some of the above-mentioned shortcomings. We fabricated a FET based biosensor using an easily operating nozzle-jet

ACCEPTED MANUSCRIPT

printer in which the source and drain electrodes consist of printed silver [52] and a transistor channel is composed of hydrothermally grown ZnO NRs on printed ZnO quantum dots seed layer forming a semiconducting interconnected network suitable for high enzyme immobilization. In general, with this simple approach we show nozzle-jet printed low-temperature processed n-channel FET device from inorganic metal oxide like widely compatible ZnO on PET substrate for glucose detection.

2. Experimental details

2.1. Reagents

Zinc acetate dihydrate [$Zn(CH_3COO)_2.2H_2O$], zinc nitrate hexahydrate [$Zn(NO_3)_2.6H_2O$, 99%], potassium hydroxide (KOH, 96%), hexamethylene tetramine (HMTA), Nafion (5 wt%), phosphate buffered saline (PBS, pH 7.4), ethanol, methanol, ethanolamine, ethylene glycol, glucose (D-(+)-99.5%), uric acid (UA), ascorbic acid (AA), lactose, cholesterol, mannose, fructose and dopamine were purchased from Sigma-Aldrich and used as received without further purification. Deionized (DI) water was exclusively used in all aqueous solutions and rinsing procedure.

2.2. Synthesis and characterization of ZnO QDs and NRs

ZnO QDs were synthesized using 0.01 M $Zn(CH_3COO)_2.2H_2O$ in methanol under vigorous stirring and heating. At 62 ºC, 0.5 M NaOH prepared in methanol was added to above solution and final pH of the solution was maintained at ~10, followed by vigorous stirring and heating for 30 min. After completion of the reaction, the resultant product was washed with methanol by centrifugation in order to remove by-products and stored in the same solvent (5 mg in 15 mL methanol). Later, for printing purpose highly

ACCEPTED MANUSCRIPT

dispersive ZnO QDs precursor ink was prepared in methanol/ethanol/ethylene glycol/ethanolamine in the ratio of 4:16:1:1 mL by volume, following sonication. To grow ZnO NRs, nozzle-jet printed ZnO seed substrates were suspended upside down into a Pyrex glass bottle containing an equal molar (0.05 M) of Zn $(NO_3)_2$. $6H_2O$ and HMTA in 50 mL DI water. Then, the sample containing solution was heated on a heating mantle for 4.5h at 80 ºC. Finally, the electrodes were rinsed and dried at room temperature.

The morphological investigation of as-synthesized ZnO QDs/NRs were observed using field-emission scanning electron microscopy (FESEM, Hitachi S4700) equipped with energy dispersive spectroscopy (EDS), transmission electron microscopy (TEM) and high-resolution TEM (HRTEM) equipped with digital charge-coupled device (JEOL JEM-2010 equipped with CCD camera). CS-Corrected-FETEM/STEM images were carried out using CS-Corrected-field emission transmission electron microscope/STEM with an acceleration voltage of 200 kV. A commercial Nozzle-Jet Printer (System Engineering Solution (SES, Korea) was used for all printing experiments. The surface roughness of nozzle-jet printed ZnO QDs seed on PET was measured using atomic force microscopy (AFM, Multimode-8, Bruker, Santa Barbara, CA, USA) at resonance frequency of 0.5 Hz (tapping mode). The cross-section of the ZnO seed layer was confirmed by focused ion beam (FIB) technique. X-ray diffraction (XRD, Rigaku) was utilized with Cu-Kα radiation (λ=1.54178 Å) to examine the crystallinity of as-synthesized ZnO QDs in the range of $10\text{-}90^0$ with 8°/min scanning speed. Moreover, ZnO QDs precursor ink was characterized by Fourier transform infrared (FTIR) spectroscopy.

2.3. Fabrication of FET based glucose sensors and measurements

ACCEPTED MANUSCRIPT

The fully printed FET based biosensor was fabricated using nozzle-jet printer on a pre-cleaned PET substrate; schematic illustrating nozzle-jet printed FET biosensor fabrication process is shown in Fig. 1. The commercial nozzle-jet printer used for printing the FET device, was operated with different nozzle tip diameters and at separate base-plate temperatures for printing silver and ZnO QDs inks. The different parameters such as, nozzle moving speed, stage temperature, air pressure, and working distance were digitally controlled. For silver ink printing, the nozzle tip of 100 µm diameter was selected and base-plate temperature was perpetuated at 80 °C, while as, for ZnO QDs ink printing, the nozzle tip of 70 µm diameter was utilized and base-plate temperature was maintained at 120 ^{0}C. First, two separate silver lines of ~800 nm thickness were printed on PET by nozzle-jet printing technique, followed by post sintering at 90 ºC. The source-drain electrodes were printed in such a way to have the channel length of 0.4 cm. Similarly, semiconductor channel of ZnO QDs ink was printed between silver lines and post sintered at 120 ^{0}C, which has a channel width of 0.5 cm and thickness of ~600 nm. Then, the ZnO NRs were grown by hydrothermal process as explained earlier. Before immobilization of enzyme (glucose oxidase; GOx), the printing based ZnO NRs FET biosensor was double rinsed with PBS (100 mM, pH 7.4) to generate hydrophilic surfaces. The enzyme solution was prepared by dissolving GOx (1.0 mg/mL) in 100 mM PBS and 5 µL of enzyme solution was dropped to immobilize the enzyme onto the surface of ZnO NRs by a physical adsorption method. After dropping enzyme solution on ZnO NRs FETs, the device was kept at 4 ºC for 12h, which allowed enzyme molecules to get absorbed onto the ZnO NRs surfaces and rinsed to remove unabsorbed enzyme. 1 µL of 0.5 wt% Nafion solution was used to cover enzyme immobilized ZnO NRs surface to

ACCEPTED MANUSCRIPT

prevent enzyme leakage and avoid interferences. Finally, PDMS was coated at the silver line and ZnO NRs interface to avoid solution contact with the silver electrode during all experimental *I-V* measurements.

The electrical properties of fabricated FET based biosensor was evaluated under air-ambient conditions with a semiconductor parameter analyzer (HP 4155A). To determine the sensing properties of the fabricated biosensors, the drain current (I_D) was measured with a fixed drain-source voltage (V_{DS} = 0.1 V) while sweeping the different gate voltage range (V_G). The V_G was applied via an Ag/AgCl reference gate electrode immersed in the solution. All the sensing measurements were conducted in 100 mM PBS (pH 7.4) at room temperature while the measuring time was 10s.

3. Results and discussion

3.1. Morphological characterization of ZnO QDs/NRs

Fig. 2 illustrates the FESEM images of the nozzle-jet printed Ag source-drain (a-c) and ZnO QDs seed layer (d-f) lines, as-grown ZnO NRs (g, h) and after GOx immobilization (i, inset). Low and high resolution of Ag source-drain and ZnO QDs seed lines exhibit smooth surface morphology. The FIB cross-sectional image shows printed Ag line thickness of ~800 nm (c). The surface FESEM view of as-grown ZnO NRs shows that the NRs are uniformly and densely grown on the seeded area (g) and length of nanorods are ~1 µm (h). Importantly, NRs were grown vertically in such a pattern forming mesh like structure leaving cage like holes at the NRs base, which becomes a suitable factor for effective enzyme trapping during immobilization process. The GOx

ACCEPTED MANUSCRIPT

immobilized ZnO NRs FESEM image confirms the uniform immobilization all over the electrode area.

Fig. 3 manifests highly crystalline low (a) and (b) high magnification Cs-TEM images, (c) FFT image, (d) SAED pattern, (e) EDS spectrum, and (f) XRD pattern of ZnO QDs. As shown in Fig. 3a and 3b, the synthesized ZnO QDs are ~10 nm in diameter and have uniform morphology. The FFT image shows the regular lines of crystal lattice of ZnO QDs, with an interplanar lattice spacing of 0.26 nm (c), corresponding to the (002) plane of hexagonal ZnO, which indicates that one of the growth planes of ZnO QDs is along the (002) plane.. The SAED and corresponding IFFT pattern (d, inset) confirms the crystalline nature and the diffraction pattern well-suites with the hexagonal wurtzite ZnO [27]. The EDS spectrum (e) clarifies purity of ZnO QDs, showing only zinc oxide phase without any impurity elements. The high crystallinity of the ZnO QDs is further confirmed by XRD analysis of ZnO QDs (f). XRD pattern of the ZnO QDs includes seven diffraction peaks at 2 (degrees) screening angles of 31.85^0, 34.07^0, 36.42^0, 47.77^0, 57.27^0, 62.18^0, and 67.87^0 are respectively indexed as (100), (002), (101), (102), (110), (103), and (112) planes, which are again in excellent agreement with the hexagonal wurtzite structure of ZnO [53].

Fig. 4 justifies 2 dimensional (a) and 3 dimensional (b) AFM analysis of the nozzle-jet printed ZnO QDs seed line on PET substrate annealed at 120 ºC showing excellent surface morphology with a route mean square roughness (RMS) value of ~5.54 nm. This observation is further supported by scrutinizing the same surface area with Gwyddion software, which also exhibits nearly same RMS value of 5.10 nm (Fig. 4c). The information about roughness average (Ra: 2.93 nm), waviness average (Wa: 2.74 nm)

ACCEPTED MANUSCRIPT

and texture of the seed layer is also emancipated by this software, showing thus very smooth and regular surface morphology. Fig. 5 shows low (a) and high (b) magnification TEM images, HRTEM (c), FFT and SAED pattern (d) of ZnO NR. The latter clearly shows the ZnO fringe plane (0001) with an inter-planar spacing of ~0.52 nm, which confirms the single crystallinity and preferential growth in the [0001] direction. The typical SAED pattern for the corresponding ZnO NR (d) along with HRTEM image suggests that the ZnO NR growth is along the [0001] direction, which is the polar c-axis of the ZnO crystal lattice.

Fig. 6 shows the FT-IR spectrum of ZnO QDs precursor ink. The broad peak at 3300 cm^{-1} corresponds to the stretching vibration of hydroxyl groups. The peaks at 2950 cm^{-1} and 2882 cm^{-1} belong to the C-H stretching modes of vibration. The peaks at 1380 cm^{-1} and 1083 cm-1 are due to bending moods of N-H and C-N stretch. Similarly, the C-O group shows stretching peak at 1047 cm^{-1}. N-H group exhibits peak at 878 cm^{-1} is due the out of plane bending absorption. The peak at 627 cm^{-1} is due the of Zn-O stretching absorption. All this observation, i.e. change in intensity and value from the corresponding normal peaks suggest well dispersion of the ZnO QDs in the ink.

3.2. Detection of glucose using FET sensor

Fig. 7 shows the schematic illustration of mechanism of redox reaction and generation of electrons (a) and circuit diagram of FET biosensor (b). In a typical redox reaction [12], glucose gets oxidized to gluconolactone in the presence of GOx (O) while GOx (O) itself gets reduced to GOx (R). The GOx (R) further reacts with the dissolved oxygen in solution, which forms GOx (O) and hydrogen peroxide (H_2O_2). The liberated H_2O_2 is quantitatively detected on the electrode through electro-oxidation process. In this

ACCEPTED MANUSCRIPT

biosensor, ZnO NR channel acts as a good conduction pathway because of its high electron affinity. Thus, the electrons generated from the enzymatic reactions on the surface of each NR pass directly through the NRs to the seed layer to the electrode. To study the response of the proposed solution-gated ZnO NR nozzle-jet printed FET biosensor, the sensor response (I_D) was recorded with an optimized and constant bias potential range in the absence/presence of 5 mM of glucose in 100 mM PBS solution (Fig. 8a). The current value substantially increases in the presence of glucose compared to that of without glucose. The enhanced current response is to the enzymatic reactions of the GOx with the glucose molecules in the presence of oxygen. The enzymatic reactions temporarily change the protonation state of conducting ZnO NRs and thus affect the I_D (drain current) with increasing V_G (gate voltage). The chemical reactions for enzymatic catalysis of glucose by GOx and oxidation of hydrogen peroxide (H_2O_2) have been illustrated in Fig. 7a.

To explore the sensing properties of the fabricated nozzle-jet printed flexible FET biosensor, experiments have been conducted under optimal conditions. The detection of glucose was carried out by measuring the I_D-V_G responses of the biosensor, as shown in Fig. 8b. It is evident that the current increases with increasing glucose concentration. This is attributed to an increase in ion concentration and fast catalytic reaction. The noticeable current changes for glucose are obtained at a higher potential range i.e. 2.0-5.0 V. The increase in current in this range is further used for plotting the calibration curve of biosensor response by taking the average of currents over the range of potentials (Fig. 8c). The calibration plot has been used for the calculation of sensitivity and linear range, which are the two vital indicators of sensing performance of any biosensor. From the plot,

ACCEPTED MANUSCRIPT

a linear behavior was obtained in the concentration range of 0.0-80 mM for glucose detection with a high regression coefficient value (R^2 = 0.9976). The nozzle-jet printed FET biosensors show a high sensitivity of 22.3 μAcm^{-2} mM^{-1} and a low limit of detection of 0.07 mM for glucose, calculated by dividing the slope of current-concentration plot (S) with the standard deviation (SD) of response. The Lineweaver-Burk plot (Fig. 8d), gives a low value of Michaelis-Menten constant (0.65 mM), which confirms strong affinity of the immobilized enzyme for glucose detection. Comparing our result with previously reported biosensors, we obtained wide linear detection range for glucose measurement (Table 1). Importantly, the previously designed glucose biosensors are mostly based on electrochemical techniques requiring potentiometry, amperometry, voltammetry, and electrochemical impedance spectroscopic measurements. However, there are some limitations of these techniques. For example, not all the protein analytes/samples are intrinsically capable of serving as redox partners in electrochemical reactions. Hence, a suitable label must be introduced in order to enhance the electrochemical reaction of the analyte on working electrodes for their detections. Moreover, these assays not only require sample dilution but also are quite expensive. However, for easy operation of these sensor chips in laboratories and at home or development of wearable and implantable device, the chip size should be reduced for real-time measurements. Note-worthy, using our FETs approach; we can also enhance the detection sensitivities by the use of amplification.

3.3. Stability and reproducibility of the sensor device

The long-term stability and reproducibility of the nozzle-jet printed flexible FET biosensor were also accessed by repetitive measurements (i.e. once a day for 8 weeks)

ACCEPTED MANUSCRIPT

using electrodes fabricated in same conditions. Overall, the biosensor shows high stability for repetitive measurements and retains about 94% of its original response after 56 times of measurements during 56 days storage for glucose detection. A little decrease in response may be due to the loss of immobilized enzyme or loss of bioactivity with repetitive use and rinsing. The reproducibility test of the nozzle-jet printed flexible FET biosensors was measured by fabricating eight electrodes in similar fabrication conditions and measuring their response in the presence of 5 mM glucose in 100 mM PBS solution. The nozzle-jet printed flexible FET biosensors showed a relative standard deviation (RSD) of ~3.4% in the glucose sensing response, which confirms good reproducibility of the nozzle-jet printed flexible FET biosensors.

3.4. Selectivity test

For selectivity determination of the nozzle-jet printed flexible FET biosensors, three glucose containing solutions were prepared in PBS buffer (one containing only 5 mM glucose and other two containing 5 mM glucose solutions with 0.1 mM (low) and 0.5 mM (high) concentrations of each electroactive agents (AA, UA, cholesterol, mannose, lactose, fructose, and dopamine) were prepared in 100 mM PBS buffer (pH 7.4). Additionally, to compare the result with real human serum sample, 5 mM glucose containing human serum sample (analyzed using commercial glucose estimation kit (CHOD-PAP method)) was used. The current response was recorded using I_D-V_G measurements and shown in Fig. 9(a). The calibrated response is shown as histogram in Fig. 9(b). The sensing response of the nozzle-jet printed flexible FET biosensor in glucose only sample, other two samples with electroactive agents showed slight decrease in the response. Importantly, low concentrations of electroactive species showed

ACCEPTED MANUSCRIPT

negligible effect on the sensing performance of biosensor, suggesting potential for the selective glucose detection. However, the sensor response decreased by ~15% in the human serum samples. The decrease in the biosensor response in human serum sample is due to presence of protein fragments and other small molecules [56]. These molecules restrict the diffusion of glucose into immobilized enzyme; thereby decrease the response of the biosensor. Further, we tested the reusability of the biosensor after rinsing used electrodes in serum samples with PBS. The results showed that the sensor recovers most of its response when it was tested in buffer solution [56].

4. Conclusion

In summary, we developed a nozzle-jet printed FET biosensor with GOx enzyme immobilized on vertically grown ZnO NRs. The ZnO NR printed FET biosensors exhibited wide linear detection range for glucose with high sensitivity and low limit of detection. We experimentally observed that nozzle-jet printed FET biosensors show almost negligible interference in PBS. Impressively, the concentrations determined by the fabricated biosensor for glucose (including the calculated interference caused during measurements) were well-matched with those of the pre-analytically determined. Thus, this approach has a great potential to reduce the test cost not only for biomedical research but also for patients suffering from glucose related disorders/diseases. Additionally, nozzle-jet printing provides a facile, environmentally-friendly, low-cost, computer-automated and layer-by-layer deposition process, which may have an enormous impact in future for rapid fabrication of sensing electrodes.

ACCEPTED MANUSCRIPT

Acknowledgements

This work was supported by the National Leading Research Laboratory program through the National Research Foundation (NRF) (NRF-2016R1A2B2016665) of Korea funded by the Ministry of Science, ICT & Future Planning. Authors also thank KBSI, Jeonju branch for SEM analysis and Mr. Jong-Gyun Kang, Center for University Research Facility (CURF) for taking good quality TEM images.

References

[1] J. Wang, Electrochemical glucose biosensors, Chem. Rev. 108 (2008) 814-825.

[2] World Health Organization (WHO). Global Report on Diabetes, 2016.

[3] K. Tian, M. Prestgard, A. Tiwari, A review of recent advances in nonenzymatic glucose sensors, Mater. Sci. Eng. C 41 (2014) 100-118.

[4] E. Renard, Implantable closed-loop glucose-sensing and insulin delivery: the future for insulin pump therapy, Curr. Opin. Pharmacol. 2 (2002) 708-716.

[5] S. F. Clarke, J. R. Foster, A history of blood glucose meters and their role in self-monitoring of diabetes mellitus, British. J. Biomed. Sci. 69 (2012) 83-93.

[6] N. C. Shah, O. Lyandres, J. T. Walsh, M. R. Glucksberg, R. P. Van Duyne, Lactate and sequential lactate-glucose sensing using surface-enhanced Raman spectroscopy, Anal. Chem. 79 (2007) 6927-6932.

[7] A. Baba, P. Taranekar, R. R. Ponnapati, W. Knoll, R. C. Advincula, Electrochemical surface plasmon resonance and waveguide-enhanced glucose biosensing with N-alkylaminated polypyrrole/glucose oxidase multilayers, ACS Appl. Mater. Interf. 2 (2010) 2347-2354.

[8] B. Fang, A. Gu, G. Wang, W. Wang, Y. Feng, C. Zhang, X. Zhang, Silver oxide nano walls grown on Cu substrate as an enzyme less glucose sensor, ACS Appl. Mater. Interf. 12 (2009) 2829-2834.

ACCEPTED MANUSCRIPT

[9] O. S. Kwon, S. H. Lee, S. J. Park, J. H. An, H. S . Song, T. Kim, J. H. Oh, J. Bae, H. Yoon, T. H. Park, J. Jang, Large-scale graphene micropattern nano-biohybrids: high-performance transducers for FET-Type flexible fluidic HIV immunoassays, Adv. Mater. 25 (2013) 4177-4185.

[10] M. I. H. Ansari, S. Hassan, A. Qurashi, F. A. Khanday, Microfluidic-integrated DNA nanobiosensors, Biosens. Bioelectron. 85 (2016) 247-260.

[11] R. Freeman, R. Gill, I. Willner, Following a protein kinase activity using a field-effect transistor device, Chem. Commun. 33 (2007) 3450-3452.

[12] E. S. Forzani, H. Zhang, L. A. Nagahara, I. Amlani, R. Tsui, N. Tao, A conducting polymer nanojunction sensor for glucose detection. Nano Lett. 4 (2004) 1785-1788.

[13] J. Janata, M. Josowicz, Conducting polymers in electronic chemical sensors, Nat. Mater. 2 (2003) 19-24.

[14] A. Star, V. Joshi, T.-R. Han, M. V. P. Altoé, G. Grüner, J. F. Stoddart, Electronic detection of the enzymatic degradation of starch, Org. Lett. 6 (2004), 2089-2092.

[15] A. Goldoni, L. Petaccia, S. Lizzit, R. Larciprete, Sensing gases with carbon nanotubes: a review of the actual situation, J. Phys.: Condens. Matter. 22 (2010) 013001.

[16] M. Bouvet, Phthalocyanine-based field-effect transistors as gas sensors, Anal. Bioanal. Chem. 384 (2006) 366-373.

[17] B. Li, D. N. Lambeth, Chemical sensing using nanostructured polythiophene transistors, Nano Lett. 8 (2008) 3563-3567.

[18] K. C. See, A. Becknell, J. Miragliotta, H. E. Katz, Enhanced response of n-channel naphthalenetetracarboxylic diimide transistors to dimethyl methylphosphonate using phenolic receptors, Adv. Mater. 19 (2007) 3322-3327.

[19] J. Huang, J. Miragliotta, A. Becknell, H. E. Katz, Hydroxy-terminated organic semiconductor-based field-effect transistors for phosphonate vapor detection, J. Am. Chem. Soc. 129 (2007) 9366-9376.

[20] J. T. Mabeck, G. G. Malliaras, Chemical and biological sensors based on organic thin-film transistors, Anal. Bioanal. Chem. 384 (2006) 343-353.

[21] S. Dutta, A. Dodabalapur, Zinc tin oxide thin film transistor sensor, Sens. Actuators B 143 (2009) 50-55.

ACCEPTED MANUSCRIPT

[22] A.-M. Andringa, C. Piliego, I. Katsouras, P. W. M. Blom, D. M. de Leeuw. NO_2 detection and real-time sensing with field-effect transistors, Chem. Mater. 26 (2014) 773-785.

[23] L. Torsi, A. Dodabalapur, Organic thin-film transistors as plastic analytical sensors, Anal. Chem. 77 (2005) 380 A-387 A.

[24] P. R. Solanki, A. Kaushik, V. V. Agrawal, B. D. Malhotra. Nanostructured metal oxide-based biosensors, NPG Asia Mater. 3 (2011) 17-24.

[25] M. M. Rahman, A. J. S. Ahammad, J.-H. Jin, S. J. Ahn, J.-J. Lee, A comprehensive review of glucose biosensors based on nanostructured metal-oxides, Sensors 10 (2010) 4855-4886.

[26] Y.-B. Hahn, R. Ahmad, N. Tripathy, Chemical and biological sensors based on metal oxide nanostructures, Chem. Commun. 48 (2012) 10369-10385.

[27] A. Qurashi, J. H. Kim, Y.-B. Hahn, Direct fabrication of ZnO nanorods array on-chip system in solution and their electrical properties, Electrochem. Commun. 18 (2012) 88-91

[28] Q. Ahsanulhaq, J. H. Kim, J. S. Lee, Y.-B. Hahn, Electrical and gas sensing properties of ZnO nanorod arrays directly grown on a four-probe electrode system, Electrochem. Commun. 12 (2010) 475-478.

[29] K. Ogata, H. Dobashi, K. Koike, S. Sasa, M. Inoue, M. Yano, Patterned growth of ZnO nanorods and enzyme immobilization toward the fabrication of glucose sensors, Physica E: Low dimens. Syst. Nanostruct. 42 (2010) 2880-2883.

[30] Y. Y. Wei, Y. Li, X. Liu, Y. Xian, G. Shi, L. Jin, ZnO nanorods/Au hybrid nanocomposites for glucose biosensor, Biosens. Bioelectron. 26 (2010) 275-278.

[31] T. Kong, Y. Chen, Y. Ye, K. Zhang, Z. Wang, X. Wang, An amperometric glucose biosensor based on the immobilization of glucose oxidase on the ZnO nanotubes, Sens. Actuators B 138 (2009) 344-350.

[32] Z. H. Dai, G. J. Shao, J. M. Hong, J. C. Bao, J. Shen, Immobilization and direct electrochemistry of glucose oxidase on a tetragonal pyramid-shaped porous ZnO nanostructure for a glucose biosensor, Biosens. Bioelectron. 24 (2009) 1286-1291.

ACCEPTED MANUSCRIPT

[33] A. Fulati, S. M. Usman Ali, M. H. Asif, N. H. Alvi, M. Willander, C. Brannmark, P. Stralfors, S. I. Borjesson, F. Elinder, B. Danielsson, An intracellular glucose biosensor based on nano-flake ZnO, Sens. Actuators B 150 (2010) 673-680.

[34] B. Fang, C. Zhang, G. Wang, M. Wang, Y. Ji, A glucose oxidase immobilization platform for glucose biosensor using ZnO hollow nanospheres, Sens. Actuators B 155 (2011) 304-310.

[35] R. Ahmad, N. Tripathy, Y.-B. Hahn, High-performance cholesterol sensor based on the solution-gated field effect transistor fabricated with ZnO nanorods, Biosens. Bioelectron. 45 (2013) 281-286.

[36] J. Li, X. Lin, Glucose biosensor based on immobilization of glucose oxidase in poly(o-aminophenol) film on polypyrrole-Pt nanocomposite modified glassy carbon electrode, Biosens. Bioelectron. 22 (2007) 2898 -2905.

[37] L. Zhu, R. Yang, J. Zhai, C. Tian, Bienzymatic glucose biosensor based on co-immobilization of peroxidase and glucose oxidase on a carbon nanotubes electrode, Biosens. Bioelectron. 23 (2007) 528-535.

[38] B. K. Shrestha, R. Ahmad, S. Shrestha, C. H. Park, C. S. Kim, In situ synthesis of cylindrical spongy polypyrrole doped protonated graphitic carbon nitride for cholesterol sensing application, Biosens. Bioelectron. 94 (2017) 686-693.

[39] R. Ahmad, N. Tripathy, M.-S. Ahn, Y.-B. Hahn, Solution process synthesis of high aspect ratio ZnO nanorods on electrode surface for sensitive electrochemical detection of uric acid, Sci. Rep. 7 (2017) 46475.

[40] S. Dasgupta, R. Kruk, N. Mechau, H. Hahn, Inkjet printed, high mobility inorganic-oxide field effect transistors processed at room temperature, ACS Nano 5 (2011) 9628-9638.

[41] T. Shimoda, K. Morii, S. Seki, H. Kiguchi, Inkjet printing of light-emitting polymer displays, MRS Bull. 28 (2003) 821-827.

[42] M. Jung, J. Kim, J. Noh, N. Lim, C. Lim, G. Lee, J. Kim, H. Kang, K. Jung, A. D. Leonard, J. M. Tour, G. Cho, All-printed and roll-to-roll-printable 13.56-MHz-operated 1-Bit RF Tag on plastic foils, IEEE Trans. Elect. Dev. 57 (2010) 571-580.

ACCEPTED MANUSCRIPT

[43] R. A. Street, W. S. Wong, S. E. Ready, M. L. Chabinyc, A. C. Arias, S. Limb, A. Salleo, R. Lujan, Jet printing flexible displays, Mater. Today 9 (2006) 32-37.

[44] T. Someya, T. Sekitani, S. Iba, Y. Kato, H. Kawaguchi, T. Sakurai, A large-area, flexible pressure sensor matrix with organic field-effect transistors for artificial skin applications, Proc. Natl. Acad. Sci. U.S.A. 101 (2004) 9966-9970.

[45] D.-H. Lee, S.-Y. Han, G. S. Hermanc, C.-H. Chang, Inkjet printed high-mobility indium zinc tin oxide thin film transistors, J. Mater. Chem. 19 (2009) 3135-3137.

[46] S. Jeong, Y.-G. Ha, J. Moon, A. Facchetti, T. J. Marks, Role of gallium doping in dramatically lowering amorphous-oxide processing temperatures for solution-derived indium zinc oxide thin-film transistors, Adv. Mater. 22 (2010) 1346-1350.

[47] C.-G. Lee, A. Dodabalapur, Solution-processed zinc tin oxide thin-film transistors with low interfacial trap density and improved performance, Appl. Phys. Lett. 96 (2010) 243501.

[48] K. Okamura, N. Mechau, D. Nikolova, H. Hahn, Influence of interface roughness on the performance of nanoparticulate zinc oxide field-effect transistors, Appl. Phys. Lett. 93 (2008) 083105.

[49] K. Okamura, N. Mechau, D. Nikolova, H. Hahn, Polymer stabilized zno nanoparticles for low-temperature and solution processed field-effect transistors, J. Mater. Chem. 20 (2010) 5651-5658.

[50] H. Faber, M. Burkhardt, A. Jedaa, D. Kälblein, H. Klauk, M. Halik, Low-temperature solution-processed memory transistors based on zinc oxide nanoparticles, Adv. Mater. 21 (2009) 3099-3104.

[51] K. Okamura, N. Mechau, D. Nikolova, H. Hahn, Influence of interface roughness on the performance of nanoparticulate zinc oxide field-effect transistors. Appl. Phys. Lett. 93 (2008) 083105.

[52] K. S. Bhat, R. Ahmad, Y. Wang, Y.-B. Hahn. Low-temperature sintering of highly conductive silver ink for flexible electronics, J. Mater. Chem. C 4 (2016) 8522-8527.

[53] H. Yu, H. Zhang, H. Huang, Y. Liu, H. Li, H. Ming and Z. Kang. ZnO/carbon quantum dots nanocomposites: one-step fabrication and superior photocatalytic ability for

ACCEPTED MANUSCRIPT

toxic gas degradation under visible light at room temperature, New J. Chem. 36 (2012) 1031-1035.

[54] K. Koike, Y. Mori, S. Sasa, Y. Hirofuji, M. Yano, Glucose sensing by an enzyme-modified ZnO-based FET, Procedia Eng. 168 (2016) 84-88.

[55] R. Ahmad, M.-S. Ahn, Y.-B. Hahn, Fabrication of a non-enzymatic glucose sensor field-effect transistor based on vertically-oriented ZnO nanorods modified with Fe_2O_3, Electrochem. Commun. 77 (2017) 107-111.

[56] R. Ahmad, N. Tripathy, J.-H. Park, Y.-B. Hahn, A comprehensive biosensor integrated with a ZnO nanorod FET array for selective detection of glucose, cholesterol and urea, Chem. Commun. 51 (2015) 11968-11971.

ACCEPTED MANUSCRIPT

ACCEPTED MANUSCRIPT

Table 1. Comparison of our nozzle-jet printed biosensor with previous reports.

Electrode	Method	Linear range (mM)	Detection limit (mM)	Sensitivity ($\mu A\ mM^{-1}\ cm^{-2}$)	Ref.
N-Alkylaminated PPy/GOx Multilayers/Au	Surface plasmon resonance	-	-	0.03	[7]
PANI-PAA/PANI-bisulfite/GOx-PDAB/Au	FET	-	-	0.001	[12]
Nafion/Au/ZnO NRs/GCE	Amperometry	0.0001-0.033	0.00001	1492	[30]
Nafion/GOx/ZnO NT	Amperometry	0.050-12	0.001	21.7	[31]
Nafion/TPSP-ZnO/GCE	Cyclic voltammetry	0.05-8.2	0.01	-	[32]
GOx/ZnO NF/Al coated on glass capilary	Potentiometry	0.0005-10	-	-	[33]
Nafion/ZnO-HNSPs/GOD/GCE	Amperometry	0.005-13.15	0.001	65.82	[34]
POAP-GOD/PPy-Pt/GCE	Amperometry	0.0015-13	0.00045	9.9	[36]
PPy/HRP-GOx/SWNT/Au	Amperometry	0.030-2.43	0.03 ± 0.009	7.01 ± 0.18	[37]
GOx-ZnO film/glass substrate	Ion-sensitive FET	0.2-40	~0.2	-	[54]
Fe_2O_3-ZnO NRs/SiO_2/Si substrate	FET	0.05-18	0.012	105.75	[55]
Nafion/GOx/ZnO NRs/Ag/PET	FET	0.0-80	0.07	22.3	This Work

ACCEPTED MANUSCRIPT

Figure captions

Fig. 1 Schematic illustration showing fabrication process of FET based biosensor.

Fig. 2 FESEM images showing surface view of printed silver line (a, b) and FIB cross-sectional (c) image. FESEM images of printed ZnO QDs line (d-f). FESEM images of vertically-grown ZnO NRs (g), cross-sectional image of ZnO NRs (h), and after GOx immobilization on ZnO NRs (i). Insets show the optical image of Ag lines on PET substrate (a) and high resolution FESEM images.

Fig. 3 CS-Corrected-FETEM/STEM images; (a) low-, (b) high-resolution, (c) FFT image, (d) SAED pattern, (e) EDS spectrum, and (f) XRD pattern of ZnO QDs.

Fig. 4 AFM analysis showing 1D (a) and 2D (b) topography of the nozzle-jet printed ZnO QDs seed line on PET and (c) root mean square (RMS) roughness.

Fig. 5 (a) Low and high magnification (inset a) TEM images, (c) HR-TEM image, and (d) FFT pattern of ZnO NR. Insets in a and d show the high magnification TEM image and SAED pattern, respectively.

Fig. 6 FT-IR spectra of ZnO QDs precursor ink. Inset shows the optical image of ink.

Fig. 7 Schematic illustrative mechanism of redox reaction (a) and circuit diagram of FET biosensor (b).

Fig. 8 Typical I_D-V_G responses of ZnO NR based printed FET biosensor without and with 5 mM of glucose in 100 mM PBS buffer (a). I_D-V_G responses with increasing glucose concentration from 0-80 mM, (b) corresponding calibration curve, i.e. response current *verses* glucose concentration (mM) in log scale with high regression coefficient (R^2) value of 0.9976 (c), and the Lineweaver-Burk plot (d).

Fig. 9 (a) Interference test of 0.5 mM glucose solution without (i), with 0.1 mM (ii) and 0.5 mM (iii) electroactive agents (AA, UA, mannose, lactose, fructose, and dopamine) and human serum sample (iv). (b) The corresponding current response is shown in the form of histogram.

ACCEPTED MANUSCRIPT

Figures

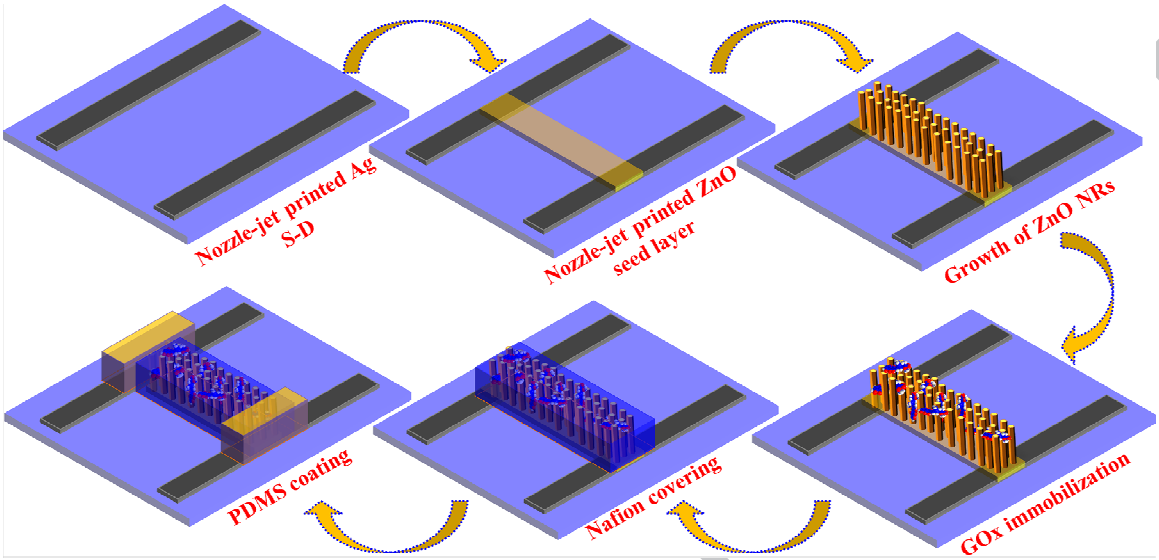

Figure 1/9

ACCEPTED MANUSCRIPT

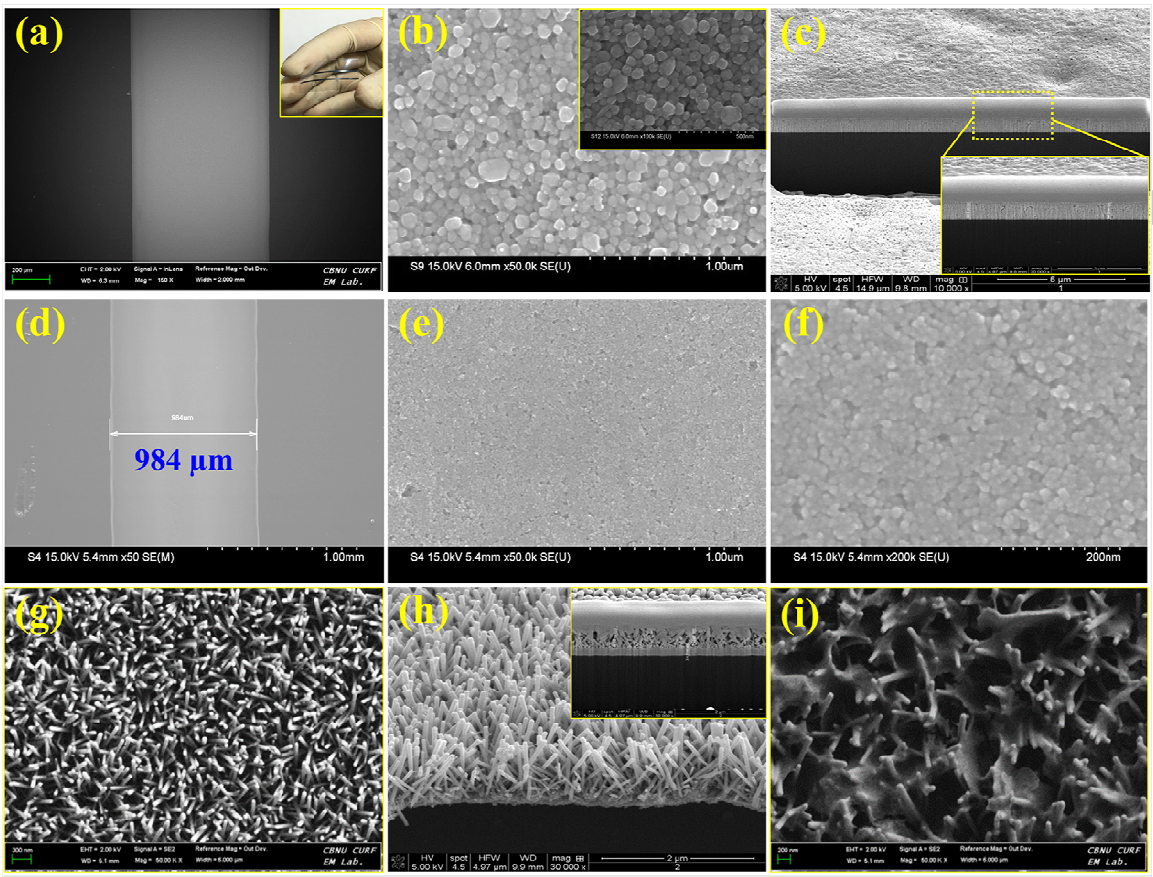

Figure 2/9

ACCEPTED MANUSCRIPT

ACCEPTED MANUSCRIPT

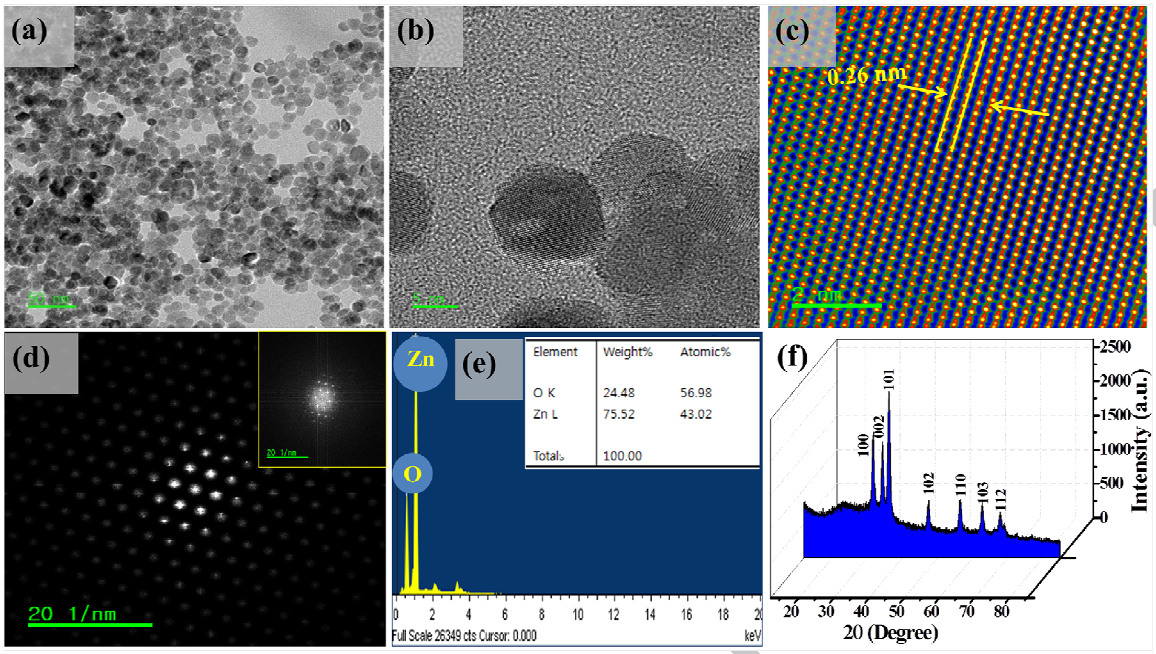

Figure 3/9

ACCEPTED MANUSCRIPT

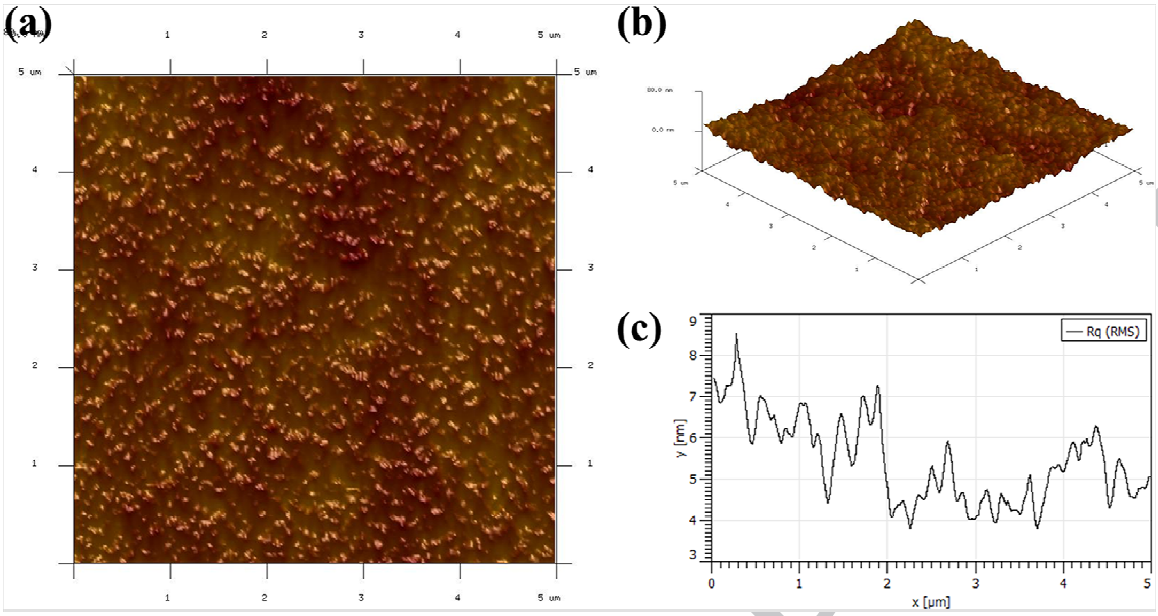

Figure 4/9

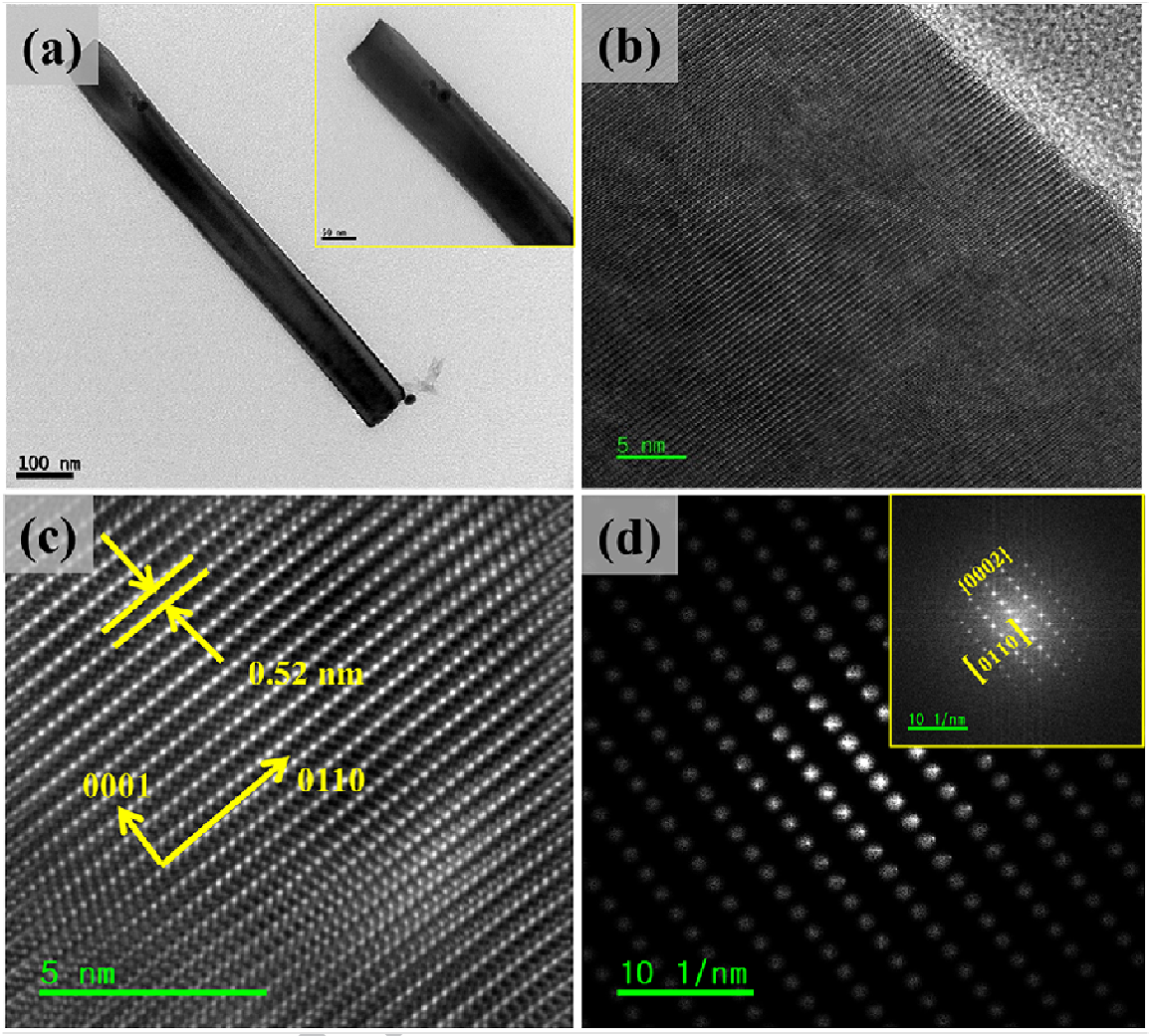

Figure 5/9

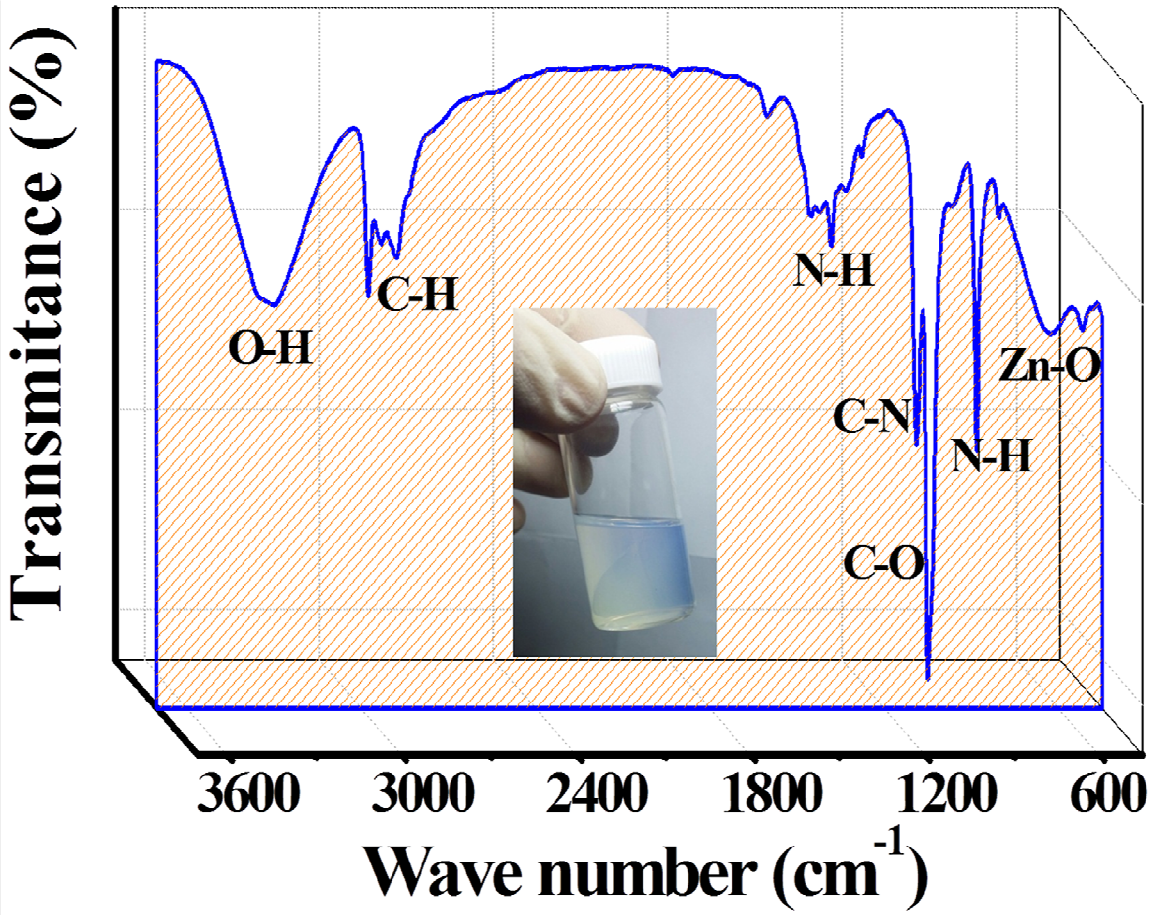

Figure 6/9

ACCEPTED

ACCEPTED MANUSCRIPT

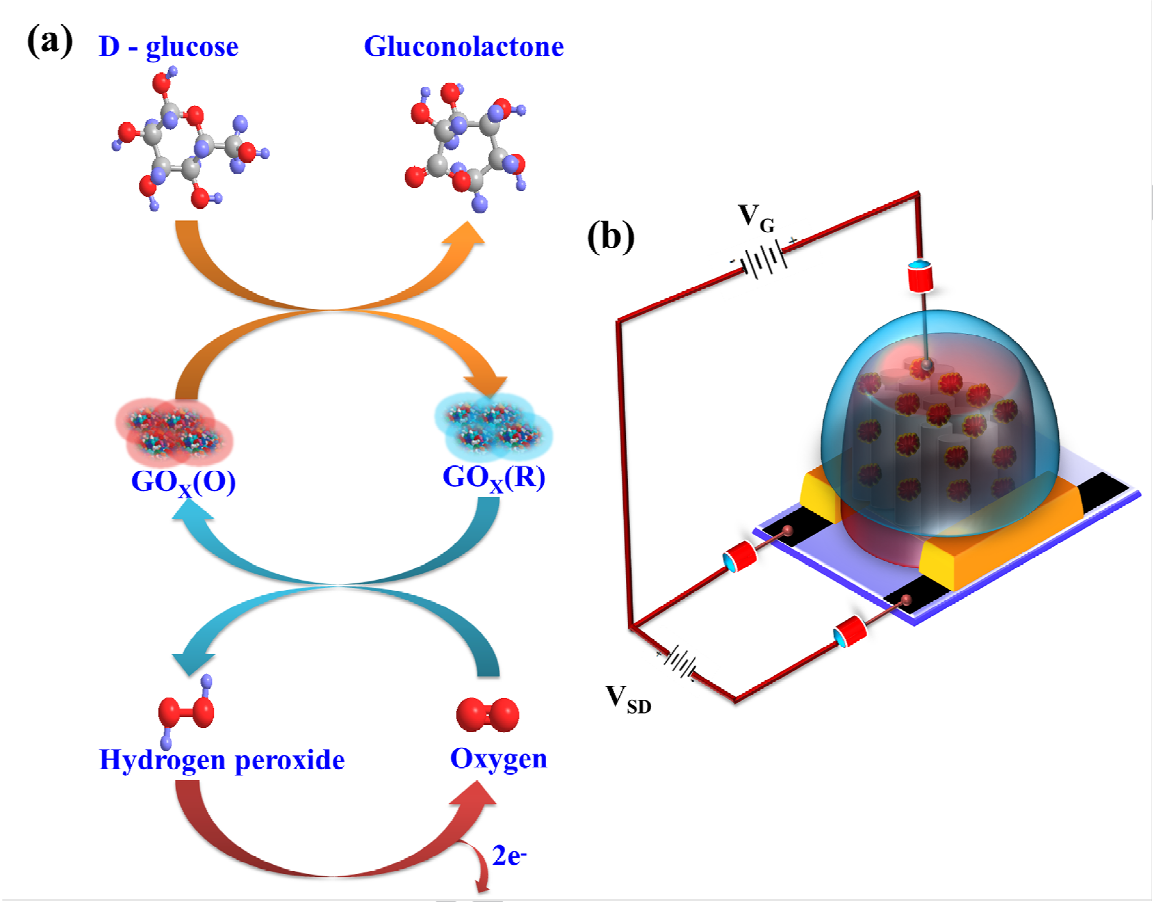

Figure 7/9

ACCEPTED

ACCEPTED MANUSCRIPT

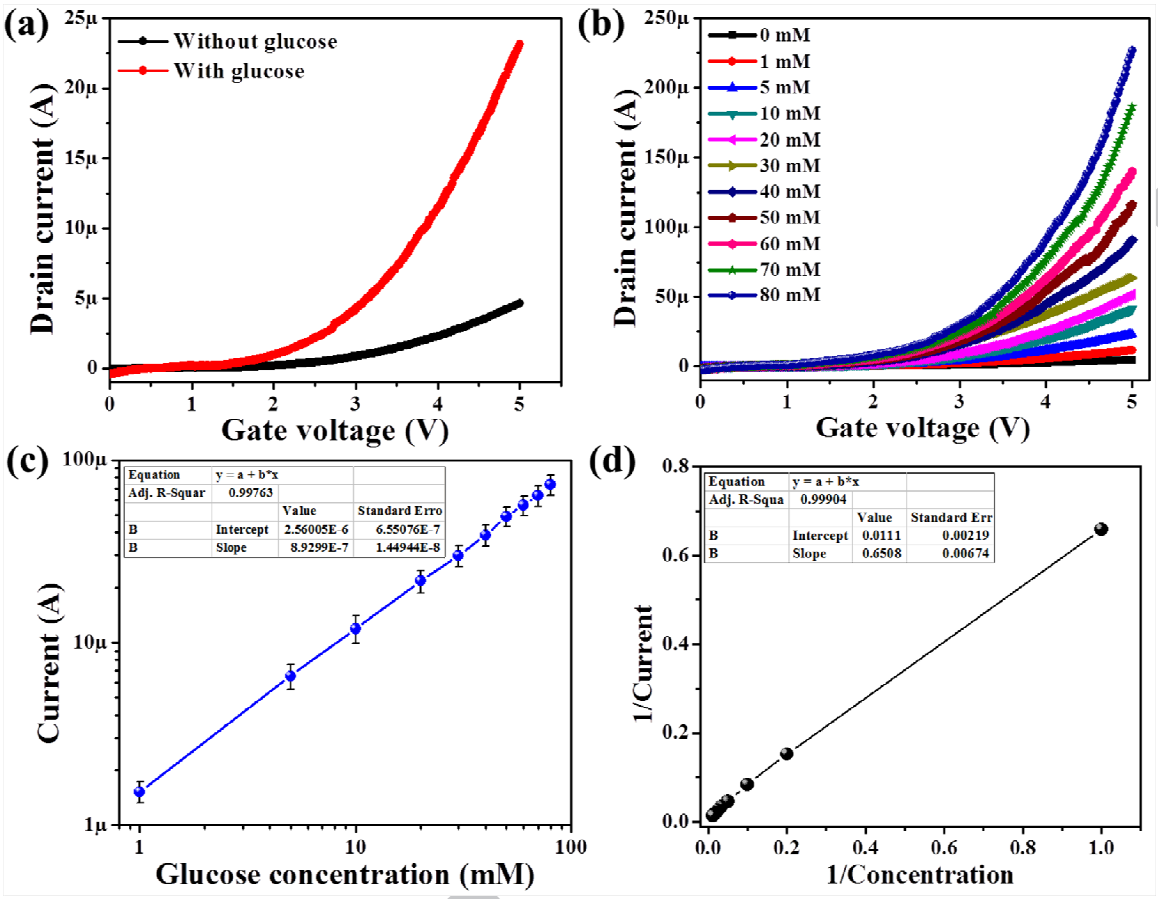

Figure 8/9

ACCEPTED

ACCEPTED MANUSCRIPT

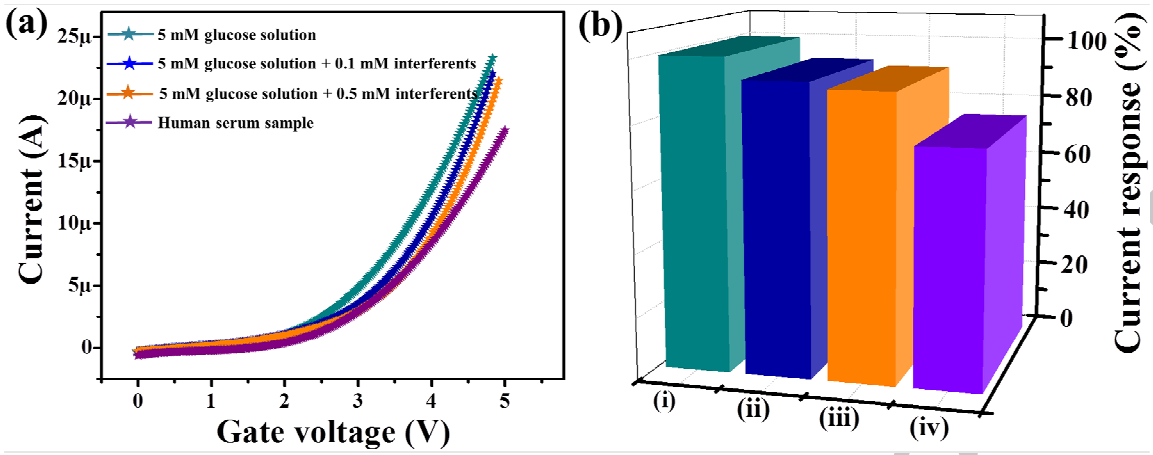

Figure 9/9

ACCEPTED MANUSCRIPT

Highlights

- Nozzle-jet printing of silver source-drain electrodes and ZnO seed layers on flexible substrate.
- Use of nozzle-jet printer resulted in high reproducible sensing active area.
- Growth of well-defined vertical ZnO NRs for high enzyme loading and enhanced sensing performance.
- Sensor showed wide glucose detection range, long-term stability and excellent reproducibility.

ACCEPTED MANUSCRIPT

ACCEPTED MANUSCRIPT

Graphical abstract

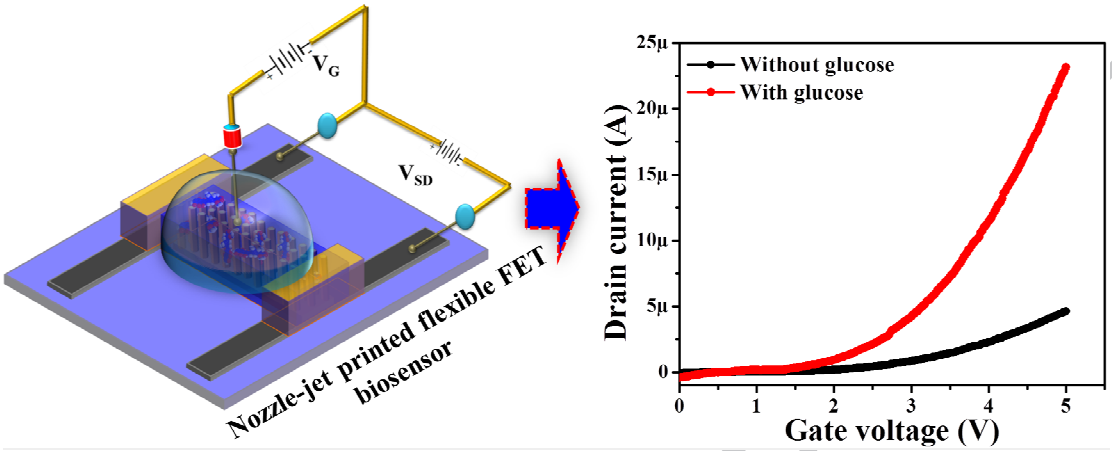

ACCEPTED MANUSCRIPT